Preparation of molecular surfaces for mesh-free Wavelet Galerkin numerical solvers

Maharavo Randrianarivony

Institute of Computer Science
Christian-Albrecht University of Kiel, Germany

September 6, 2007

Abstract: We want to transform molecular surfaces which are in the form of Van der Waals model into a structure which is acceptable by mesh-free Wavelet solvers. In this document, we concentrate on the generation of spherical patches by using rational Bézier surfaces and homogeneous coordinates. Our main emphasis is that we can achieve global continuity between two patches without using approximations. Our method of attaining exact global continuity is based on the generalized stereographic projection. In that way, a spherical patch with circular boundaries can be exactly determined in a linear setting. Since we need parametric representations, we describe briefly the various steps to convert the initial CSG representation into B-Rep structure. In addition to theoretical descriptions, we report on the practical decompositions of a few molecular surfaces.

1 Introduction

Computer modeling of chemical phenomena has grown very rapidly in the last years [16, 29, 3]. In particular, the modeling of interaction between solute and solvent has received a lot of attention. The use of Boundary Element Method (BEM) for treating similar problems numerically is now well established [17, 18]. There are already a lot of works in the domain of mesh-based approaches [23, 29] in numerical chemical modeling. That does not only concern simulation methods but also preparation of geometries by using meshes. Algorithms and softwares for meshing of molecular surfaces are now well established [5]. In contrast to mesh-based approaches, modeling of molecular surfaces for use in mesh-free simulation is not yet well developed. That situation still prevails nowadays although the efficiency of mesh-free methods have been theoretically demonstrated a number of times.

In this document, we want to contribute in the development of geometric algorithms for preparation of mesh-free geometries. The method that we use here is an application of the methods that we introduce in [27]. While we used approximation to obtain global continuity in [28] for CAD objects, we are able to achieve *exact* global continuity for molecular surfaces in this document. As a result, the error analysis which has been done in [28] is irrelevant here. That is due to the fact that both circular arcs and spherical patches can be exactly represented as conics [33] and quadrics. Thus, the use of rational Bézier setting supplies an exact representation of those two entities which are the only occurring geometric entities in molecular surfaces.

In the next section, we will give a motivation from chemistry where we will show the occurrence of an integral equation problem from electric distribution of charges. We will also briefly describe the treatment of such problem with the help of Wavelet Galerkin scheme. In section 3, we will see the common approach of representing molecular surfaces and we will describe the problem precisely. In section 4, we describe the way of obtaining the B-rep structure of a given molecular surface. From the set of spheres, we need to derive the vertices, edges and faces of the B-Rep structure. Additionally, the parametrizations of the faces are required in order to do the decomposition from a planar domain to the molecular surface. We recall in section 5 the decomposition of a closed surface into a set of four-sided surfaces. The most interesting part of this paper is in section 6 where we exactly show how to parametrize the four-sided spherical patches while having global continuity in mind. The presented method in this document resembles the one in [1] where rational triangular Bézier patch of second degree are treated. The main difference is that we have tensor product rectangular Bézier patches where we take global continuity into consideration. That remark applies also to [25] where more general surfaces like cyclides are used. At the end of the paper, we present some decomposition of a few molecular surfaces and we point out some interesting problems which we will treat in the future. We note that the results of the geometric structure here can equally be used for other schemes like panel-clustering [17, 18] because we have mappings starting from the 2D unit square which can serve as generation of hierarchical structure from 2D to 3D.

2 Motivation from computational chemistry

In this section, we will describe briefly the occurrence of an integral equation problem in the domain of electrostatic interactions [3]. For two charge distributions ρ_1 and ρ_2, the electrostatic potentials V_1 and V_2 verify the

relation:

$$\forall\, \mathbf{x} \in \Omega, \qquad -\mathrm{div}(\varepsilon(\mathbf{x})\nabla V_k(\mathbf{x})) = 4\pi\rho_k(\mathbf{x}), \qquad k = 1, 2, \tag{1}$$

where $\varepsilon(\mathbf{x})$ is 1 inside the cavity Ω while it is equal to the macroscopic dielectric constant ε of the solvent outside Ω. The boundary of Ω represents the solute-solvent boundary which is in our case the molecular surface. The solvent is represented by a continuous dielectric medium while the solute is located inside the cavity Ω. The interaction energy is defined as

$$E_s(\rho_1, \rho_2) = \int_{\mathbf{R}^3} \rho_1 V_2 = \int_{\mathbf{R}^3} \rho_2 V_1 = \int_{\mathbf{R}^3} \varepsilon \nabla V_1 \cdot \nabla V_2. \tag{2}$$

By introducing the reaction potential

$$V_k^r := V_k - \phi_k, \qquad k = 1, 2, \tag{3}$$

where ϕ_k is the electrostatic potential verifying $-\Delta\phi_k = 4\pi\rho$, the charge interaction verifies

$$\begin{array}{lcll} -\Delta V^r & = & 0 & \text{in} \quad \Omega \\ -\Delta V^r & = & 0 & \text{in} \quad \mathbf{R}^3 \setminus \bar{\Omega} \\ V^r & \to & 0 & \text{at infinity} \\ [V^r] & = & 0 & \text{on} \quad S \end{array} \tag{4}$$

where $[V^r]$ represents the jump through the surface boundary $S = \partial\Omega$. By using the single layer potential

$$V^r(\mathbf{x}) = \int_\Gamma \frac{\sigma(\mathbf{y})}{\|\mathbf{x} - \mathbf{y}\|} d\mathbf{y} \qquad \forall\, \mathbf{x} \in \mathbf{R}^3, \tag{5}$$

we obtain the following integral equation

$$a(\mathbf{x})\sigma(\mathbf{x}) - \int_\Gamma \frac{\partial}{\partial n_{\mathbf{x}}} \left(\frac{1}{\|\mathbf{x} - \mathbf{y}\|} \right) \sigma(\mathbf{y}) d\mathbf{y} = h(\mathbf{x}), \tag{6}$$

where the unknown is the function σ while the nonzero quantities $h(\mathbf{x})$ and $a(\mathbf{x})$ depend exclusively on ϕ and $\varepsilon(\mathbf{x})$ respectively. The ASC approach or Apparent Surface Charge method is the way of solving the above chemical problem by searching for the solution of the integral equation in (6). Nowadays, the ASC approach is the most used method for treating this problem.

Without loss of generality, we may suppose that the coefficient $a(\mathbf{x})$ of equation (6) is unity by dividing everything by $a(\mathbf{x})$. By representing the integral in (6) with the help of an operator $\mathcal{K}$, we can introduce a second operator $\mathcal{A}$ defined by

$$(\mathcal{A}f)(\mathbf{x}) := f(\mathbf{x}) + (\mathcal{K}f)(\mathbf{x}) \qquad \forall\, \mathbf{x} \in S. \tag{7}$$

We obtain therefore the variational formulation consisting in searching for $u \in H^{1/2}(S)$ such that

$$(\mathcal{A}u, v)_S = (f, v)_S \qquad \forall v \in H^{1/2}(S)\,. \tag{8}$$

In general, the approximation scheme consists in considering a finite dimensional space R_h where we approximate the function u by $u_h \in R_h$ in which we solve the following problem

$$(\mathcal{A}u_h, v_h)_S = (f, v_h)_S \qquad \forall v_h \in R_h. \tag{9}$$

The Wavelet-Galerkin scheme [19, 9] requires that the boundary surface S be split into several foursided patches F_i such that there is a regular mapping

$$\gamma_i : [0,1]^2 \longrightarrow F_i. \tag{10}$$

Basically, the construction of wavelets on the manifold S is performed in three steps. First, wavelets are defined on the unit interval $[0, 1]$. Then, a tensor products method is used to obtain wavelets on the unit square $[0, 1]^2$ from the results on the unit interval. Finally, we use parametric lifting with the help of the parametric function γ_i to carry the results from the unit square over to the manifold F_i. The resulting wavelet spaces are used to generate the finite dimensional space R_h in relation (9).

3 Problem setting

In terms of computer simulation, each constituting atom in a molecule is represented as an imaginary sphere. The radius of each sphere corresponds to the Van der Walls radius of the atom [34]. In the domain of numerical modelings, there are currently three kinds of method for representing molecular surfaces. First, a VWS model or Van der Waals Surface [34] is composed of the trimmed spherical surfaces which are obtained from the boundaries of the constituting atoms. That is, a Van der Waal surface is simply the boundary surface of the union of the atoms as in Fig. 1(a). Second, the Solvent-Accessible Surface or SAS model is similar to the VWS model but the radii of the atoms are enlarged by a constant factor. Finally, the Solvent-Excluded Surface or SES representation sets the whole molecular surface in form of a smooth surface with G^1-joints at all intersurfaces. That is achieved by inserting toroidal blend between two spherical patches belonging to two different atoms. This last kind of surface is also known as 'Smooth Molecular Surface' or 'Connolly Surface'.

For the Wavelet-Galerkin mesh-free method, we will develop a technique for preparing molecular surfaces which are given in VWS models. To that end, let us denote by $\mathcal{B}(\omega, \rho)$ the closed ball of center ω and radius ρ:

$$\mathcal{B}(\omega, \rho) := \left\{\mathbf{x} \in \mathbf{R}^3 :\ \mathrm{dist}(\omega, \mathbf{x}) \leq \rho\right\}. \tag{11}$$

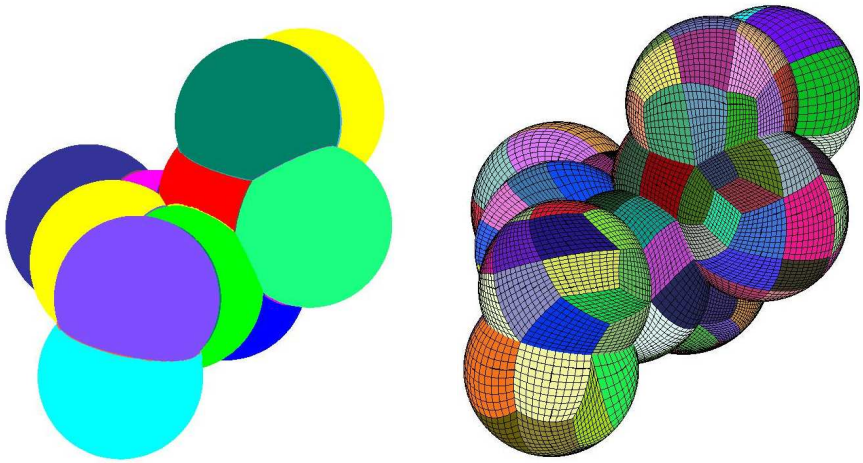

(a) (b)

Figure 1: (a)Spherical surfaces (b)Decomposition into foursided surfaces.

Consider N balls $\mathcal{B}_k := \mathcal{B}(\Omega_k, \rho_k)$ whose union forms one connected region. The molecular surface is the boundary of the union of those balls

$$S := \partial \left[\bigcup_{k=1}^{N} \mathcal{B}_k \right], \tag{12}$$

which represents a closed surface.

Since we want to treat molecular surfaces so that they can be used for Wavelet-Galerkin mesh-free simulations as explained in (9) and (10), we need to tessellate the surface S into m four-sided domains F_i

$$S = \bigcup_{i=1}^{m} F_i, \tag{13}$$

where the splitting is conforming. That is to say, every two different nondisjoint patches F_i and F_j share either a complete edge or a single corner. We need also some regular functions γ_i such that

$$F_i = \gamma_i([0,1]^2). \tag{14}$$

Additionally, we require global continuity which means that for two adjacent patches F_i and F_j, there is a bijective mapping A such that

$$\gamma_i(s) = \gamma_j(A(s)) \qquad \forall s \in \partial[0,1]^2. \tag{15}$$

In order to keep the subsequent computational cost of integral equation solvers low, it is advantageous if the number m of foursided patches from (13) is small.

A graphical illustration of the surface decomposition can be found in Fig. 1(b) where we can clearly observe that two adjacent patches have the above matching condition (15) at the interface. The decomposition algorithm follows mainly the approaches in [27] which we will summarize in section 5. We have already developed [28] a general geometric method for splitting a closed surface into foursided patches. We can certainly apply that method here but the main particularity in molecular surfaces is that it is possible to generate the mappings in (14) where the global continuity is *exact* as opposed to the approximation in [28].

4 B-rep of molecular surfaces

The description of the molecular surface S as in relation (12) is good for CSG where the only required geometric primitives are spheres. Since B-Rep structure using parametrizations for the faces is more convenient for the surface decompositions, we have to convert that CSG representation into B-rep structure. That is, we need to find explicitly the set of edges, vertices and faces whose parametrization serves as lifting from planar decompositions.

4.1 Edges and vertices of the model

In order to find the edges which are circular arcs, the intersections of the spheres $\mathcal{B}_k$ need to be determined. If two spheres are not disjoint, their intersection is a circle. Thus, the first step in the generation of the B-rep structure is the determination of the circles of intersections $\mathcal{C}_i$ of non-disjoint spheres as seen in Fig.2(b). Consider two spheres $\mathcal{B}(\omega_1, R_1)$ and $\mathcal{B}(\omega_2, R_2)$ where we suppose $R_1 \geq R_2$ and let ρ be the distance between the centers where $\rho < R_1 + R_2$. The 3D circle of intersection is uniquely determined by its center, radius and the normal vector of the plane containing the circle. The center of the desired circle of intersection is

$$\omega := \omega_1 + D\vec{U} \qquad \text{where} \qquad D := \frac{R_1^2 - R_2^2}{2\rho} + \frac{\rho}{2} \tag{16}$$

while its radius and normal vector are given by $r := \sqrt{R_1^2 - D^2}$ and $\vec{U} := \overrightarrow{\omega_1\omega_2}/\|\omega_1\omega_2\|$.

After finding all the circles of intersections $\mathcal{C}_i$, we determine the circular arcs which represent the edges of the B-Rep structure and which are part of the circles $\mathcal{C}_i$. So as to find those circular arcs, we make intersections of the circles. Note that two intersecting nonidentical circles residing on the same sphere have two points of intersections. Now, we would like to describe how to efficiently compute the intersections of two 3D circles $\mathcal{C}_1$ and $\mathcal{C}_2$ which

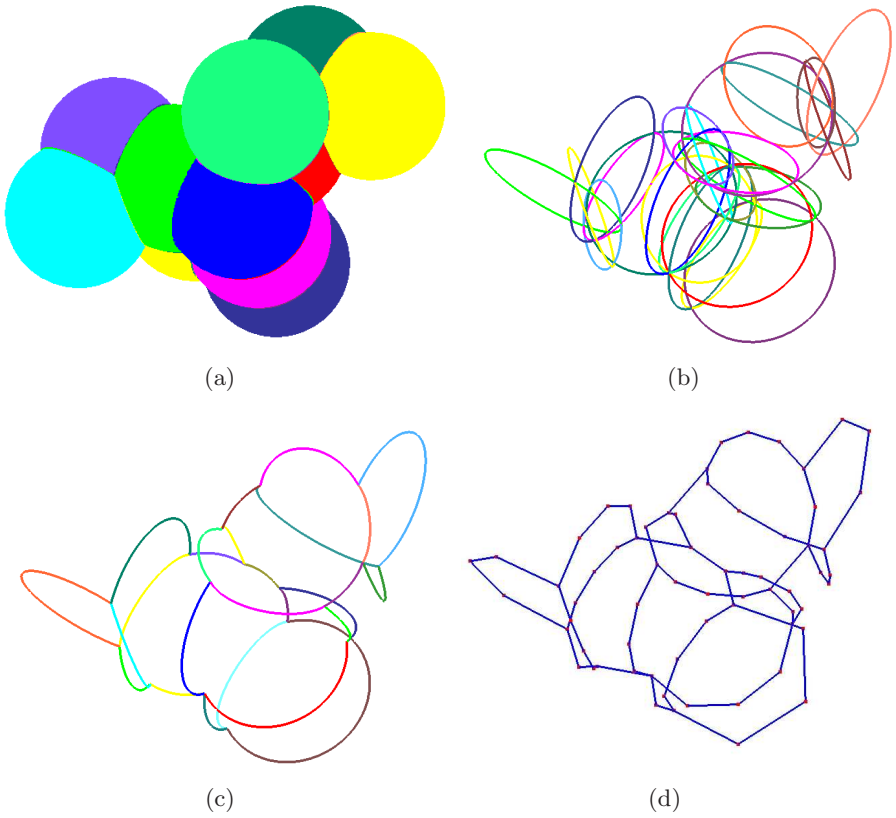

Figure 2: (a)Set of spheres (b)Circles of intersections (c)Circular arcs as edges of the B-Rep model (d)Piecewise-Linear approximation.

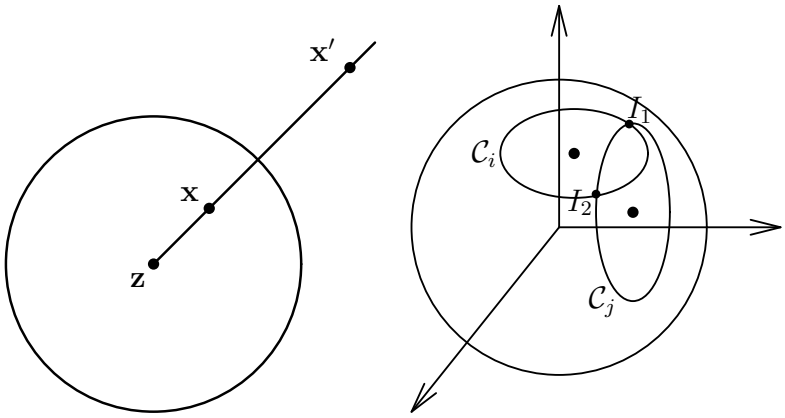

Figure 3: (a)Inversion mapping (b)3D circle-circle intersection.

reside on a sphere $\mathcal{B}$. For that, we make use of the inversion mapping Ψ_Σ with respect to a sphere Σ of center $\mathbf{z}$ and radius ρ:

$$\Psi_\Sigma : \mathbf{x} \mapsto \frac{\rho}{\|\mathbf{zx}\|^2}(\mathbf{x} - \mathbf{z}) + \mathbf{z}. \tag{17}$$

Let us first recall two properties of the inversion map [6] which is illustrated in Fig. 3(a). The inversion mapping Ψ_Σ transforms a sphere passing through the center of inversion $\mathbf{z}$ to a plane. Additionally, the image of a plane is a sphere passing through $\mathbf{z}$. Now let us suppose that the sphere $\mathcal{B}$ passes through the origin. We want to use the inversion map Ψ_Σ with respect to a sphere Σ whose center $\mathbf{z}$ is the origin. Since the circle $\mathcal{C}_k$ $(k = 1, 2)$ is located on the sphere $\mathcal{B}$, it must be the intersection of a plane $\mathcal{P}_k$ and the sphere $\mathcal{B}$. Due to the above properties of the inversion map, $\Psi_\Sigma(\mathcal{B})$ is a plane which we denote by $\mathcal{Q}$ while $\Psi_\Sigma(\mathcal{P}_1)$ and $\Psi_\Sigma(\mathcal{P}_2)$ are spheres. As a consequence, the images $\Psi_\Sigma(\mathcal{C}_k)$ are 2D circles c_k on the plane $\mathcal{Q}$. The 2D circles c_1 and c_2 intersect at the two points $I_1, I_2 \in \mathcal{Q}$ which are very easy to compute exactly because they are on a plane. Since the inverse Ψ_Σ^{-1} is Ψ_Σ itself, the intersections of the 3D-circles $\mathcal{C}_1$, $\mathcal{C}_2$ are $\Psi_\Sigma(I_1)$ and $\Psi_\Sigma(I_2)$.

The set of those points of intersections which constitutes the vertices of the B-rep structure splits the circles $\mathcal{C}_i$ into a set of circular arcs $\mathcal{A}_i$. As a next step in the assembly of the B-Rep structure, we sort the circular arcs $\mathcal{A}_i$ in order to reject those which are not useful. A circular arc which is not between two spherical patches should be removed. As a consequence, a circular arc $\mathcal{A}_i \subset \mathcal{B}_p$ which resides within a certain sphere $\mathcal{B}_k$ with $k \neq p$ should be rejected. That can be detected by taking the midpoint M_i of $\mathcal{A}_i$ and by testing whether M_i is strictly inside $\mathcal{B}_k$. When all useless arcs are removed, the remaining arcs describe the edges of the B-rep of the molecular surface as illustrated in Fig. 2(c).

4.2 Faces of the model and their parametrizations

In order to complete the B-rep structure and to use it in the surface decomposition, we need to find its faces together with their parametrizations. For each sphere $\mathcal{B}_k$, the circular arcs which are incident upon it split the sphere $\mathcal{B}_k$ into subsurfaces $G_{k,i} \subset \mathcal{B}_k$ where $i = 0, ..., p_k$. By removing the subsurfaces $G_{k,i} \subset \mathcal{B}_k$ which are contained inside other spheres $\mathcal{B}_p$ with $p \neq k$, the set of the remaining subsurfaces forms the spherical faces Γ_j of the B-Rep structure. At this position, we suppose that we have a set of N spherical surfaces Γ_k such that their union forms the molecular surface S from (12)

$$S = \cup_{k=0}^{N} \Gamma_k. \tag{18}$$

Additionally, we assume that each surface Γ_k which is not necessarily foursided is bounded by some circular arcs $\mathcal{A}_i$. That is, there is some set of indices η_k such that

$$\partial\Gamma_k = \cup_{i\in\eta_k} \mathcal{A}_i \qquad \forall\, k = 1, ..., N. \tag{19}$$

Now, we want to represent each surface Γ_k as parametric trimmed surface defined on some planar domain. Our aim is to represent such parametrization with the help of the usual stereographic projection σ [24]. Towards that end, we need to be able to find the preimage $\mathbf{y}$ of a given rational Bézier curve $\mathbf{x}$ by the stereographic projection σ. Suppose that the curve $\mathbf{x}$ is given in homogeneous coordinates as

$$\mathbf{x}(t) = \sum_{i=0}^{n} [\omega_i : \omega_i x_i : \omega_i y_i : \omega_i z_i] B_i^n(t). \tag{20}$$

A few computations reveal that the following curve maps to $\mathbf{x}$ by σ

$$\mathbf{y}(t) = \sigma^{-1}[\mathbf{x}(t)] = \begin{bmatrix} \sum_{i=0}^{n} (\omega_i - \omega_i z_i) B_i^n(t) \\ \sum_{i=0}^{n} \omega_i x_i B_i^n(t) \\ \sum_{i=0}^{n} \omega_i y_i B_i^n(t) \\ 0 \end{bmatrix} = \begin{bmatrix} \sum_{i=0}^{n} \tilde{\omega}_i B_i^n(t) \\ \sum_{i=0}^{n} \tilde{\omega}_i \tilde{x}_i B_i^n(t) \\ \sum_{i=0}^{n} \tilde{\omega}_i \tilde{y}_i B_i^n(t) \\ 0 \end{bmatrix} \tag{21}$$

where $\tilde{\omega}_i := \omega_i(1 - z_i)$ and $\tilde{\mathbf{b}}_i := (\tilde{x}_i, \tilde{y}_i, 0) := (x_i/1 - z_i, y_i/1 - z_i, 0)$. In other words, the preimage curve of $\mathbf{x}$ is the rational Bézier curve

$$\mathbf{y}(t) = \frac{\sum_{i=0}^{n} \tilde{\omega}_i \tilde{\mathbf{b}}_i B_i^n(t)}{\sum_{i=0}^{n} \tilde{\omega}_i B_i^n(t)}. \tag{22}$$

In the above description, we excluded the useless case where the value of each z_i is unity. That situation is impractical because it describes a curve which degenerates into the point $(0, 0, 1)$ on the unit sphere $\mathbf{U}$.

Let us denote by σ_k the analogue of the stereographic projection σ with respect to a sphere $\mathcal{B}_k$ from (12) which is not necessarily centered at the origin and whose radius is not generally unity. By using the above method, we can search for the preimage $\mathcal{E}_j$ of each circular arc $\mathcal{A}_j \subset \mathcal{B}_k$ with $j \in \eta_k$. Each preimage $\mathcal{E}_j^k$ is a planar curve defined from some interval $[e_j^k, f_j^k]$. Let $\mathcal{D}_k$ be the planar trimmed domain bounded by $\mathcal{E}_j$ for $j \in \eta_k$. Thus, we have a trimmed surface

$$\sigma_k : \mathcal{D}_k \longrightarrow \mathcal{B}_k \quad \text{with} \quad \Gamma_k = \sigma_k(\mathcal{D}_k) \qquad \forall\, k = 1, ..., N. \tag{23}$$

5 Summary of splitting into patches

Since we have a set of trimmed parametric surfaces bounding a solid, the current situation agrees exactly with the surface structure in [27]. Therefore, we can use the decomposition technique there which we want to summarize now.

5.1 Polyhedral model

Basically, we make the four-sided splitting in a planar domain $\mathcal{D}_k$, then we lift up the results in the molecular surface by means of the parametrization σ_k. In order to do the planar decomposition, we approximate first the curved boundaries of $\{\Gamma_k\}$ by straight line segments separated by nodes $\{X_i\} \subset \mathbf{R}^3$ as in Fig. 2(d). So as to achieve that approximation while having conforming splitting in mind, we create planar polygonalizations of $\{\mathcal{D}_k\}_{k=1}^N$ which amount to doing the following. For each trimmed surface Γ_k, we generate a polygon $P^{(k)}$ whose nodes $\mathbf{x}_i^{(k)}$ are taken from the curved boundary of the 2D domain $\mathcal{D}_k$. We have to make sure that for two adjacent different surfaces Γ_k and Γ_p sharing a curve $\mathcal{C}$, if $\sigma_k(\mathbf{x}_i^{(k)}) \in \mathcal{C}$, then there must exist a vertex $\mathbf{x}_l^{(p)} \in P^{(p)}$ such that

$$\sigma_k(\mathbf{x}_i^{(k)}) = \sigma_p(\mathbf{x}_l^{(p)}). \tag{24}$$

Let us note that if we take too few vertices, the resulting polygon $P^{(k)}$ may have imperfections such that its edges do not form an admissible polygon as illustrated in Fig. 4(a). But if the polygonal approximation is too fine, then it results in overly many four-sided surfaces. As a consequence, one has to split the curved edges adaptively while trying to maintain relation (24) which involves some preimage computations. Let us emphasize that only polygons having an *even* number of boundary vertices can be decomposed into quadrilaterals. It is not straightforward to convert odd faces into even ones inside a closed surface with arbitrary genus. One should assemble the adjacency graph which is used in the Dijkstra algorithm to search for

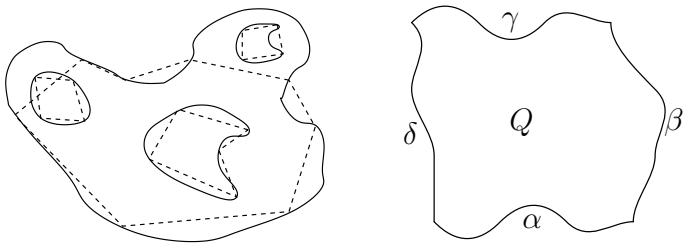

Figure 4: (a)Imperfections in polygonal approximation (b)Four-sided patch

the shortest path joining two odd polygons in order that the number of additional nodes to be inserted are not too many. We could theoretically prove that the number of odd faces must be even for a closed model –which is the case for molecular surfaces– and that the odd faces can be converted to even ones pairwise.

5.2 Quadrangulation and decomposition

We consider the polygon $P^{(k)}$ which we decompose into a set of convex quadrilaterals $q_{k,i}$. In the decomposition of a polygon $P^{(k)}$ into quadrilaterals $q_{k,i}$, we use only the preimages $\sigma_k^{-1}(X_i)$ of the nodes $\{X_i\}$ as boundary vertices. That is, we do not use any additional boundary nodes in the course of the quadrangulation process. We have developed in [27] an approach that decomposes a polygon with n boundary vertices into $\mathcal{O}(n)$ convex quadrilaterals.

Consider a convex quadrilateral $q = [a_1, a_2, a_3, a_4]$ which is a member of the quadrangulation of the polygon $P^{(k)}$. We want now to describe how to find the corresponding four-sided patch F on the sphere $\mathcal{B}_k$. The four corners of the spherical patch F are defined to be $\sigma_k(a)$, $\sigma_k(b)$, $\sigma_k(c)$, $\sigma_k(d)$. The four circular sides of F are defined as follows. Let $e_i := [a_i, a_{i+1}]$ denote the four edges of the quadrilateral q. The four circular edges f_1, f_2, f_3, f_4 of F are derived from the edges e_1, e_2, e_3, e_4 respectively. If e_j is an internal edge of $P^{(k)}$, f_j will be the circular geodesic which joins $\sigma_k(a_j)$ and $\sigma_k(a_{j+1})$ on the sphere $\mathcal{B}_k$. Otherwise, f_j will be the circular arc which is part of the boundary of Γ_k. In order to facilitate the description of the mappings in the next section, let us denote by α, β, γ, δ the planar preimages of the curved edges f_1, f_2, f_3, f_4 by the projection σ_k.

5.3 Coons and approximated global continuity

In this section we will summarize our previous method of generating a mapping from the unit square while approximating global continuity. Since our method of generating that map is based on transfinite interpolation, we briefly recall some basic facts about this technique [14, 15, 31]. Suppose that Q is delineated by four curves α, β, γ, $\delta : [0,1] \longrightarrow \mathbf{R}^2$ that fulfill the compatibility conditions at the corners:

$$\alpha(0) = \delta(0)\,, \quad \alpha(1) = \beta(0)\,, \quad \gamma(0) = \delta(1)\,, \quad \gamma(1) = \beta(1). \tag{25}$$

We assume that besides the common points in (25), there are no further intersection points as in Fig. 4(b). We are interested in generating a parametric surface $\mathbf{x}(u,v)$ defined on the unit square $[0,1]^2$ such that the boundary of the image of $\mathbf{x}$ coincides with the given four curves:

$$\begin{array}{lll} \mathbf{x}(u,0) = \alpha(u) & \mathbf{x}(u,1) = \gamma(u) & \forall\, u \in [0,1] \\ \mathbf{x}(0,v) = \delta(v) & \mathbf{x}(1,v) = \beta(v) & \forall\, v \in [0,1]\ . \end{array} \tag{26}$$

This transfinite interpolation problem can be solved by a first order Coons [20, 32] patch $\mathbf{x}$ which can be defined in matrix form as

$$\mathbf{x}(u,v) = -\begin{bmatrix} -1 \\ F_0(u) \\ F_1(u) \end{bmatrix}^T \begin{bmatrix} \mathbf{0} & \mathbf{x}(u,0) & \mathbf{x}(u,1) \\ \mathbf{x}(0,v) & \mathbf{x}(0,0) & \mathbf{x}(0,1) \\ \mathbf{x}(1,v) & \mathbf{x}(1,0) & \mathbf{x}(1,1) \end{bmatrix} \begin{bmatrix} -1 \\ F_0(v) \\ F_1(v) \end{bmatrix}. \tag{27}$$

The blending functions F_0 and F_1 denote two arbitrary smooth functions satisfying:

$$F_i(j) = \delta_{ij} \quad i,j = 0,1 \quad \text{and} \qquad F_0(t) + F_1(t) = 1 \quad \forall\, t \in [0,1]. \tag{28}$$

Our previous method was to replace the 2D curves $\mathcal{E}_i^j$ delineating the domain $\mathcal{D}_i$ that we met in (23) by $\tilde{\mathcal{E}}_i^j$ so that they have the same shapes $\mathrm{Im}(\mathcal{E}_i^j) = \mathrm{Im}(\tilde{\mathcal{E}}_i^j)$ but they have different parametrizations. Let us denote by ρ_i^j the composition $\sigma_i \circ \mathcal{E}_i^j$ and let us introduce the length function

$$\chi_i^j(t) := \int_{e_i^j}^{t} \left\| \frac{d\rho_i^j}{dt}(\theta) \right\| d\theta. \tag{29}$$

This function is defined from $[e_i^j, f_i^j]$ to $[0, L]$ where L is the total length of the curve ρ_i^j. Without loss of generality we may assume that

$$\frac{d\chi_i^j}{dt}(t) = \left\| \frac{d\rho_i^j}{dt}(t) \right\| \neq 0 \qquad \forall t. \tag{30}$$

Hence, there is an inverse function $\phi_i^j := (\chi_i^j)^{-1}$ and our objective is to replace the function $\mathcal{E}_i^j$ by $\tilde{\mathcal{E}}_i^j := \mathcal{E}_i^j \circ \phi_i^j$. We could prove in [28] that if we replace the initial parametrization into chord length parametrization, then we can approximate global continuity.

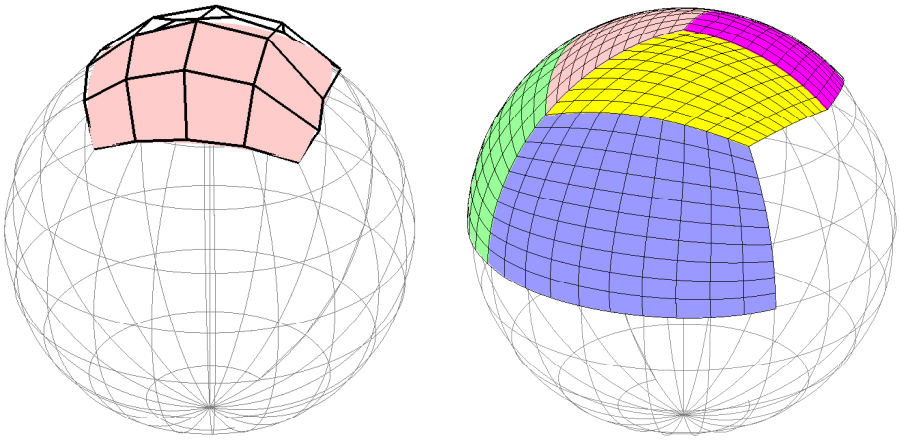

(a) (b)

Figure 5: (a)A spherical patch as rational Bézier and its control net (b)Globally continuous rational Bézier patches.

6 Four-sided spherical patches

In this section, we want to investigate the approach of generating mappings to a spherical patch without using approximation. Throughout this section, we will represent any four-sided spherical patch as rational Bézier as in Fig.5(a) for two reasons. First, all spherical patches with circular sides can be represented as rational Bézier without any approximation error. Second, one can achieve exact global continuity at the surface joints as shown in Fig.5(b). According to our experiences, spherical patches with geodesic boundary curves have very good visual looks. But the presented method works for any circular boundary: that is, each side is the intersection of a sphere and a plane. Although most of the methods here are described for the unit sphere $\mathbf{U}$ centered at the origin, they can be easily carried over to any non-degenerated sphere with minor modifications.

Since projective geometry is the most suitable method for treating rational Bézier curves and patches in our situation [6], let us introduce some relevant definitions. An element of the projective space $\mathbf{E}^3$ will be denoted as a column vector with four coordinates or as row vector whose elements are separated by columns. Thus, a point with $[w : x : y : z]$ as homogeneous coordinates will have the cartesian coordinates $(x/w, y/w, z/w)$. Using homogeneous computations simplifies theoretical formulations considerably because rational quantities become polynomial ones which make problems linear instead of nonlinear. For example, let us consider a rational Bézier curve with weights w_i and control points $\mathbf{b}_i = (x_i, y_i, z_i)$ in cartesian

coordinates:

$$\mathbf{X}(t) := \frac{\sum_{i=0}^{n} \omega_i \mathbf{b}_i B_i^n(t)}{\sum_{i=0}^{n} \omega_i B_i^n(t)}. \tag{31}$$

It corresponds to a Bézier curve having homogeneous coordinates $[\omega_i : \omega_i x_i : \omega_i y_i : \omega_i z_i]$ in projective space. In our next parametrizations, we will need the following plane

$$\mathbf{P} := \{[w : x : y : 0] \in \mathbf{E}^3 \quad \text{with} \quad w, x, y \in \mathbf{R}\} \tag{32}$$

which corresponds to the plane $z = 0$ in cartesian coordinates.

6.1 Projections in projective space

The following generation of the spherical mappings makes use of the next three projections which have been used by Dietz *et al.* in [11, 12]. First, the hyperbolic projection ϑ transforms a point $[e_0 : e_1 : e_2 : e_3]$ to a point in $\mathbf{P}$ given by

$$\vartheta(\mathbf{e}) := \left[e_0^2 + e_3^2 : e_0 e_1 - e_2 e_3 : e_1 e_3 + e_0 e_2 : 0\right]. \tag{33}$$

Second, the stereographic projection is defined from $\mathbf{P}$ to the unit sphere $\mathbf{U}$ by

$$\sigma(\mathbf{e}) = \left[e_0^2 + e_1^2 + e_2^2 : 2e_0 e_1 : 2e_0 e_2 : e_1^2 + e_2^2 - e_0^2\right]. \tag{34}$$

Finally, the generalized stereographic projection is given by

$$\delta(\mathbf{e}) = \begin{bmatrix} e_0^2 + e_1^2 + e_2^2 + e_3^2 \\ 2e_0 e_1 - 2e_2 e_3 \\ 2e_1 e_3 + 2e_0 e_2 \\ e_1^2 + e_2^2 - e_0^2 - e_3^2 \end{bmatrix}. \tag{35}$$

The relation between those three projections is $\delta = \sigma \circ \vartheta$. Since we will need to compute preimages by δ very often in molecular surface, we have explicitly computed the preimage of a point on $\mathbf{U}$ in terms of spherical coordinates (φ, θ) as follows:

$$\begin{aligned} e_0 &= \sin^2\theta \\ e_1 &= \sin\theta\cos\varphi - \sin\varphi\sin^2\theta + \sin\varphi + \sin\theta\cos\varphi\cos\theta + \cos\theta\sin\varphi \\ e_2 &= \sin\theta\sin\varphi + \sin^2\theta\cos\varphi - \cos\varphi + \cos\theta\sin\theta\sin\varphi - \cos\varphi\cos\theta \\ e_3 &= \cos\theta\sin\theta. \end{aligned} \tag{36}$$

For a point $\mathbf{q} = [q_0 : q_1 : q_2 : q_3]$ we have

$$\bar{\mathbf{q}} := [q_2 : q_3 : -q_0 : -q_1] \tag{37}$$

$$\mathbf{q}^{\perp} := [-q_3 : q_2 : -q_1 : -q_0]. \tag{38}$$

The set of preimages of a point $\mathbf{Q}$ is a projective line [11, 12]

$$\delta^{-1}(\mathbf{Q}) = \{\lambda\mathbf{q} + \mu\mathbf{q}^{\perp} : \quad \lambda, \mu \in \mathbf{R}\}, \tag{39}$$

where $\mathbf{q}$ is a preimage of $\mathbf{Q}$. The product formula

$$B_i^n(t)B_j^m(t) = \frac{\binom{n}{i}\binom{m}{j}}{\binom{n+m}{i+j}} B_{i+j}^{n+m}(t) \tag{40}$$

shows that the image by the generalized stereographic projection δ of a rational Bézier of degree n is a rational Bézier of degree $2n$ which is drawn on the unit sphere. Conversely, it has been shown [11, 12] that every irreducible spherical rational Bézier curve/surface of degree $2n$ can be represented as the image by δ of some rational Bézier curve/surface of degree n.

6.2 Circular boundary curves

In this section, we want to parametrize a circular arc with fixed endpoints as an image of the generalized stereographic projection δ. There are already plenty of methods [20, 21] for representing a circular arc as rational Bézier but we explicitly need that it is an image of δ because we intend to have global continuity as described in the next section. Toward that end, we suppose that we have four points $\mathbf{Q}_i$ belonging to a circle $\mathcal{C}$ which is contained in the unit sphere $\mathbf{U}$. We assume that those points are equispaced as illustrated in Fig. 6(a). Additionally, we are given two points $\mathbf{b}_0 \in \mathbf{E}^3$ and $\mathbf{b}_2 \in \mathbf{E}^3$ which are transformed by δ to the first and the last points: $\delta(\mathbf{b}_0) = \mathbf{Q}_0$ and $\delta(\mathbf{b}_2) = \mathbf{Q}_3$. We want to determine a conic $\mathbf{x}$ which maps by δ to the circle $\mathcal{C}$. In other words, we want to find the internal node $\mathbf{b}_1 \in \mathbf{E}^3$ such that the image of the following quadratic Bézier curve by δ is $\mathcal{C}$

$$\mathbf{x}(t) = \mathbf{b}_0 B_0^2(t) + \mathbf{b}_1 B_1^2(t) + \mathbf{b}_2 B_2^2(t) \quad \text{with} \quad \mathbf{b}_i = [w_i : x_i : y_i : z_i]. \tag{41}$$

We will show that searching for the middle point $\mathbf{b}_1$ is equivalent to solving a linear system of size four. We want that the internal points $\mathbf{Q}_1$ and $\mathbf{Q}_2$ correspond to the parameter values $t_1 := 1/3$ and $t_2 := 2/3$ as $\delta[\mathbf{x}(t_i)] = \mathbf{Q}_i$. Toward that end, we choose a preimage $\mathbf{q}_i$ of $\mathbf{Q}_i$ by δ. Since $\delta^{-1}(\mathbf{Q}_i) = \{\lambda \mathbf{q}_i + \mu \mathbf{q}_i^\perp : \lambda, \mu \in \mathbf{R}\}$, we have

$$< \bar{\mathbf{q}}_i, \mathbf{x}(t_i) >= 0, \quad \text{and} \quad < \bar{\mathbf{q}}_i^\perp, \mathbf{x}(t_i) >= 0 \tag{42}$$

which imply:

$$< \bar{\mathbf{q}}_i, \mathbf{b}_1 >= K(\bar{\mathbf{q}}_i, t_i) \qquad < \bar{\mathbf{q}}_i^\perp, \mathbf{b}_1 >= K(\bar{\mathbf{q}}_i^\perp, t_i), \qquad \text{for} \quad i = 1, 2, \tag{43}$$

where

$$K(\mathbf{q}, t) := -\frac{1}{B_1^2(t)} \left[< \mathbf{q}, \mathbf{b}_0 > B_0^2(t) + < \mathbf{q}, \mathbf{b}_2 > B_2^2(t) \right]. \tag{44}$$

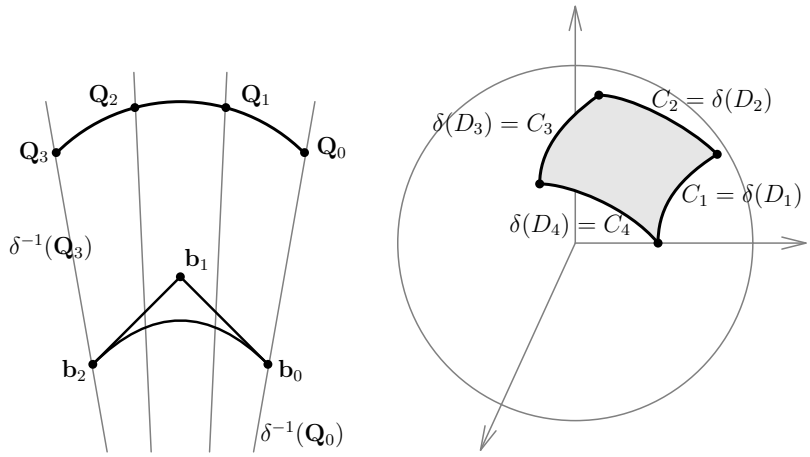

Figure 6: (a)A conic maps to the circle by δ the generalized stereographic projection (b)Spherical patch delineated by four circular arcs.

With the four homogeneous coordinates of $\mathbf{b}_1$, the relations in (43) lead to a linear system of size four. Since the curve $\mathbf{x}$ from relation (41) is a Bézier of degree two in homogeneous coordinates, its image by δ is a rational Bézier curve of degree four in cartesian coordinates.

6.3 Internal spherical patches

Let us consider four circles C_k represented as rational Bézier curves which are drawn on the unit sphere $\mathbf{U}$ and which enclose a four-sided spherical surface $\mathcal{H}$. By using several degree elevations, we can suppose that they have the same degree. Thus, the curves are supposed to have the next representation in homogeneous coordinates

$$C_k(t) = \sum_{i=0}^{2n} \mathbf{c}_i^k B_i^{2n}(t) \quad \text{with} \quad \mathbf{c}_i^k = [w_i^k : x_i^k : y_i^k : z_i^k]. \tag{45}$$

Additionally, we assume that they are the images of four Bézier curves D_k of degree n by the mapping δ as shown in Fig.6(b). That is to say, we have

$$C_k(t) = \delta[D_k(t)] \qquad \text{with} \qquad D_k(t) = \sum_{i=0}^{n} \mathbf{d}_i^k B_i^n(t) \tag{46}$$

such that there is coincidence at the corners:

$$\mathbf{d}_0^1 = \mathbf{d}_0^4, \qquad \mathbf{d}_n^1 = \mathbf{d}_0^2, \qquad \mathbf{d}_n^2 = \mathbf{d}_n^3, \qquad \mathbf{d}_0^3 = \mathbf{d}_n^4. \tag{47}$$

What we are searching is not simply a rational Bézier surface which interpolates those curves but a spherical transfinite interpolant $\mathbf{X}$ residing on $\mathbf{U}$. That is, we want to find a spherical patch $\mathbf{X}$ which pointwise interpolates those curves at the boundary:

$$\begin{array}{lll} \mathbf{X}(u,0) = C_1(u), & \mathbf{X}(u,1) = C_3(u) & \forall u \in [0,1], \\ \mathbf{X}(0,v) = C_4(v), & \mathbf{X}(1,v) = C_2(v) & \forall v \in [0,1], \\ \mathbf{X}(u,v) \in \mathbf{U} & \forall\, (u,v) \in [0,1]^2. & \end{array} \tag{48}$$

The desired patch $\mathbf{X}$ will be represented as a rational Bézier surface having the following form in homogeneous coordinates

$$\mathbf{X}(u,v) = \sum_{i=0}^{2n} \sum_{j=0}^{2n} \mathbf{b}_{ij} B_i^{2n}(u) B_j^{2n}(v) \quad \text{with} \quad \mathbf{b}_{ij} = [w_{ij} : x_{ij} : y_{ij} : z_{ij}]. \tag{49}$$

Due to the property of δ in (39) and (40), that problem amounts to searching for some rational Bézier $\mathbf{Y}$ of degree n which maps by δ to $\mathbf{X}$ as:

$$\mathbf{X}(u,v) = \delta[\mathbf{Y}(u,v)] \qquad \text{with} \qquad \mathbf{Y}(u,v) = \sum_{i=0}^{n} \sum_{j=0}^{n} \mathbf{a}_{ij} B_i^n(u) B_j^n(v). \tag{50}$$

Thus, the problem is reduced to the determination of the homogeneous control points $\mathbf{a}_{ij}$ of $\mathbf{Y}$. On account of the boundary conditions (48), the boundary control points should be chosen as

$$\mathbf{a}_{i0} := \mathbf{d}_i^1, \quad \mathbf{a}_{in} := \mathbf{d}_i^3, \quad \mathbf{a}_{0j} := \mathbf{d}_j^4, \quad \mathbf{a}_{nj} := \mathbf{d}_j^2, \quad \forall\, i,j = 0,...,n. \tag{51}$$

Hence, the task remains in determining the internal control points $\mathbf{a}_{ij}$ which are found by specifying that the image rational Bézier $\mathbf{X}$ interpolates some given internal points $Q_k \in \mathcal{H} \subset \mathbf{U}$ at $(u_k, v_k) \in [0,1]^2$:

$$\mathbf{X}(u_k, v_k) = \delta[\mathbf{Y}(u_k, v_k)] = Q_k \qquad \forall\, k = 1,...,m := 2(n-1)^2. \tag{52}$$

Let $\mathbf{q}_k$ be a preimage of Q_k by the mapping δ. We want to determine the control points $\mathbf{a}_{ij}$ such that we have the following relation:

$$\mathbf{Y}(u_k, v_k) = \mathbf{q}_k \qquad \forall\, k = 1,...,m. \tag{53}$$

As a result, we have two equalities:

$$\langle \bar{\mathbf{q}}_k, \mathbf{Y}(u_k, v_k) \rangle = 0, \qquad \langle \bar{\mathbf{q}}_k^{\perp}, \mathbf{Y}(u_k, v_k) \rangle = 0, \qquad \forall\, k = 1,...,m. \tag{54}$$

By denoting the set of indices (i,j) for internal and boundary control points of $\mathbf{Y}$ by $\mathcal{J}$ and $\mathcal{B}$ respectively, we obtain

$$\langle \bar{\mathbf{q}}_k, \sum_{(i,j)\in\mathcal{B}} \mathbf{a}_{ij} B_i^n(u_k) B_j^n(v_k) + \sum_{(i,j)\in\mathcal{J}} \mathbf{a}_{ij} B_i^n(u_k) B_j^n(v_k) \rangle = 0. \tag{55}$$

$$\sum_{(i,j)\in\mathcal{J}} \langle \bar{\mathbf{q}}_k, \mathbf{a}_{ij}\rangle B_i^n(u_k)B_j^n(v_k) = -\langle \bar{\mathbf{q}}_k, \sum_{(i,j)\in\mathcal{B}} \mathbf{a}_{ij} B_i^n(u_k)B_j^n(v_k)\rangle. \qquad (56)$$

We can repeat the same computations in order to obtain similar relations for $\bar{\mathbf{q}}_k^{\perp}$. Since the control points $\mathbf{a}_{ij}$ for $(i,j) \in \mathcal{B}$ are specified by (51), the right hand side of (56) is completely known. Therefore, this leads to some linear system of equations having $\mathbf{a}_{ij}$ with $(i,j) \in \mathcal{J}$ as unknowns.

7 Implementations and future works

We have implemented routines in C/C++ and OpenGL in order to split molecular surfaces into patches. Although the conversion of the CSG representation into a B-rep structure is not very theoretically sound as described in section 4, its implementation constitutes a large part of the program. Three examples of decomposition into four-sided surfaces can be seen in Fig. 7, Fig. 8 and Fig. 9. They correspond to molecules of propane, pentane and ice which have respectively 11, 17 and 84 atoms. The final decompositions have respectively 231, 388 and 1284 four-sided patches as observed in Fig. 7(b), Fig. 8(b) and Fig. 9(b).

Until now we have already implemented a lot of programs about decomposition and mappings. Still, the size of the problem is not yet large because we made only the programmings for illustration purpose. We have treated molecular surfaces consisting of no more than 90 atoms. That is, we have concentrated more on the implementation of the theoretical methods than on the speed and efficiency of the programs. In the future, we plan to extend our geometric routines to be able to handle real world molecules that have over 200 atoms as illustrated in Fig. 10. Our ultimate objective is to treat extremely large molecules like proteins with thousands of atoms.

Apart from the size of the problem, two important points will be investigated more carefully. First, spheres which are almost tangent to each other create difficulty in the splitting method because the resulting trimmed surfaces become very tight and curved in the neighborhood of the tangency. More theoretical works might still be necessary to examine the properties of the mappings from the unit square to a patch which is long and thin. That situation might not happen for small molecules such as benzene or fullerene but it almost always occurs for large molecules. Second, we have mainly treated problems where one sphere generates a single trimmed surface. If we have several trimmed surfaces from one sphere, we should improve the detection routine in order to find the trimmed surfaces more efficiently.

On the other hand, we want to improve the method of loading the initial input. It would be advantageous if we have completely automatic routines

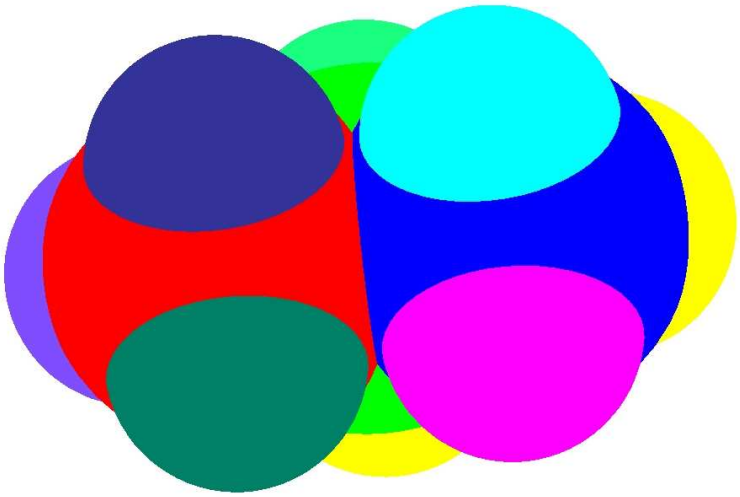

(a)

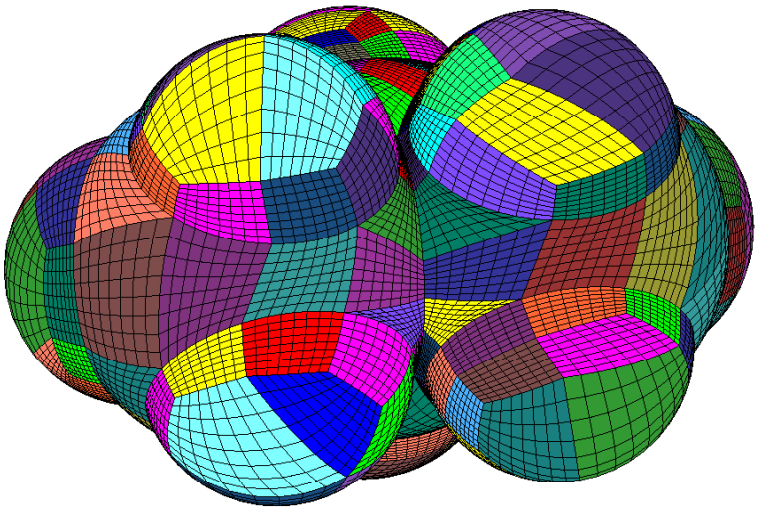

(b)

Figure 7: (a)Propane molecule with 11 atoms (b)Decomposition with 231 four-sided patches.

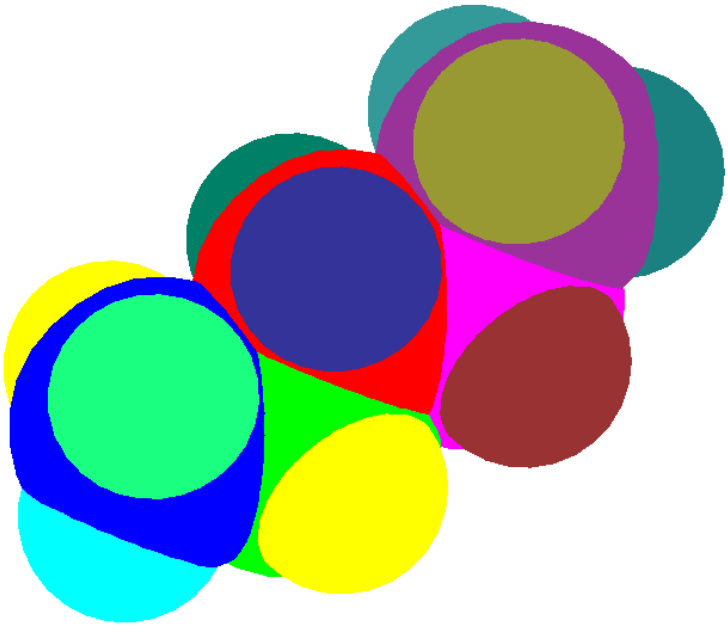

(a)

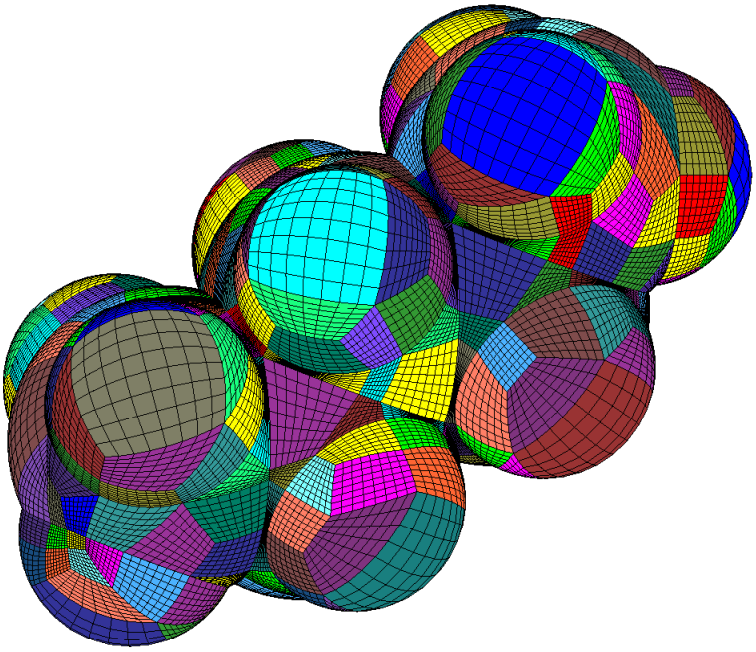

(b)

Figure 8: (a)Pentane molecule with 17 atoms (b)Decomposition with 388 four-sided patches.

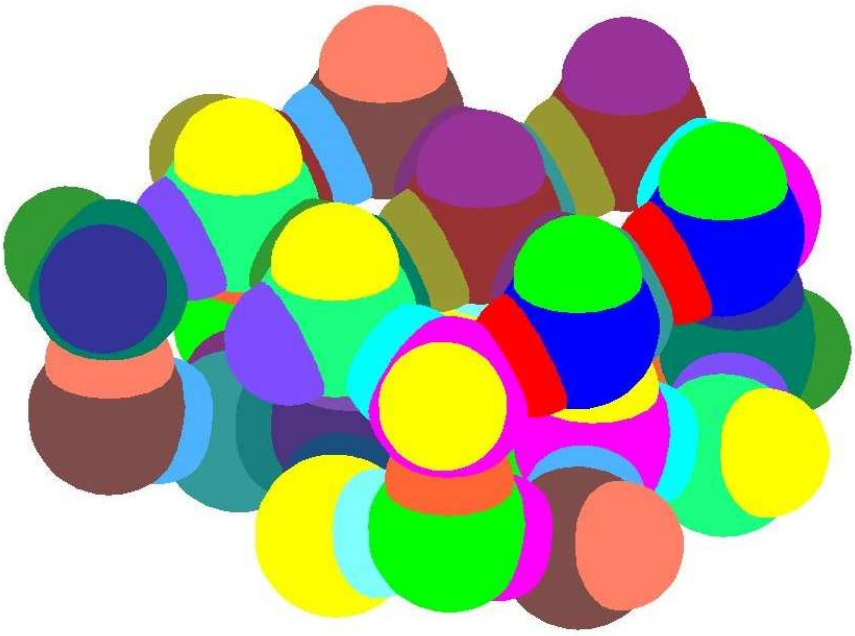

(a)

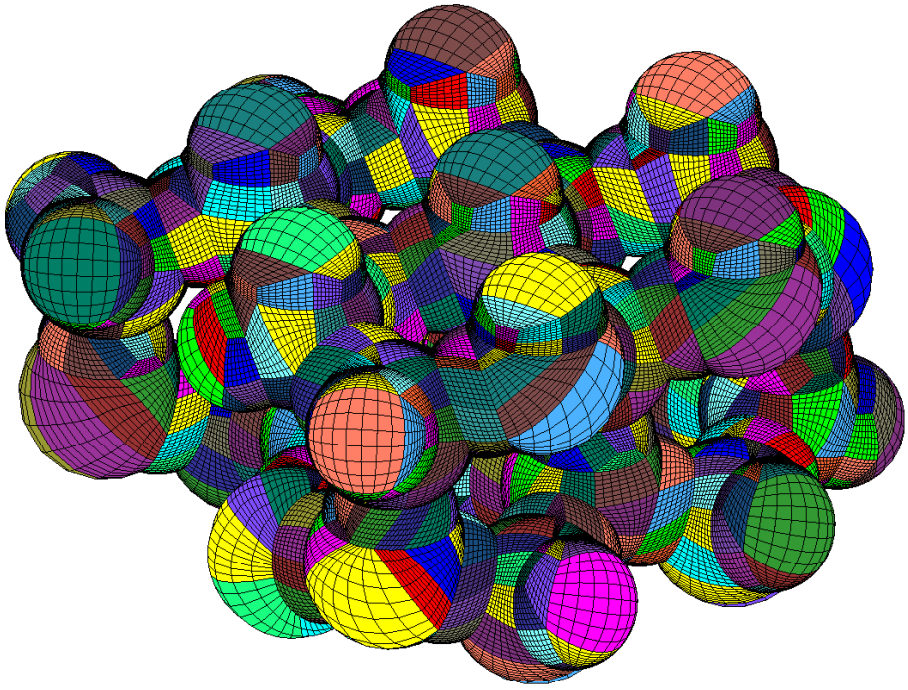

(b)

Figure 9: (a)Ice molecule with 84 atoms (b)Decomposition with 1284 four-sided patches.

for treating any PDB files (Protein Data Bank) which are the usual standards to digitally store chemical entities. That is helpful to reduce manual operations for sorting out important relevant information from files having large molecules like DNA or proteins which usually have between 500 to several thousands of atoms.

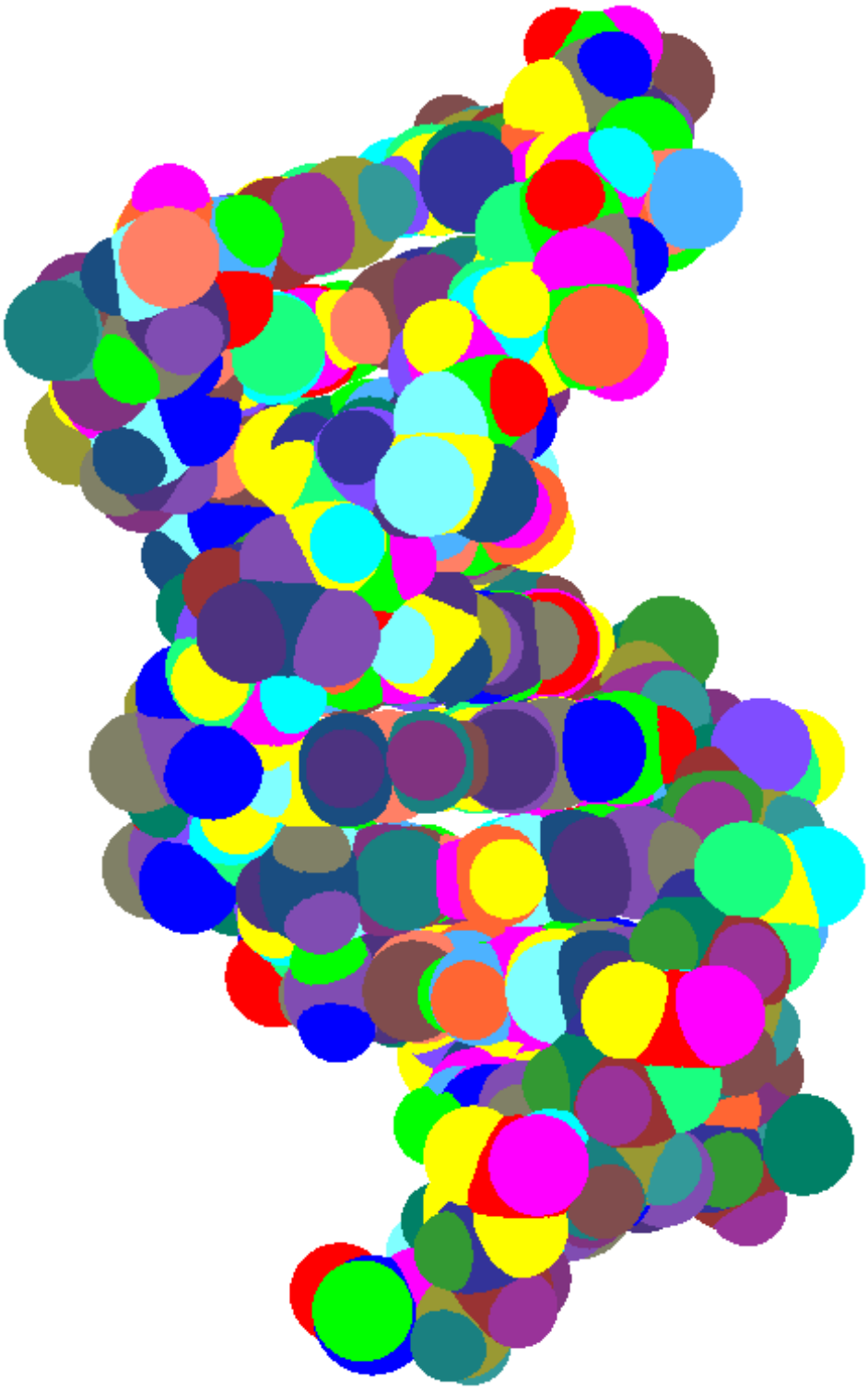

Figure 10: Future work: DNA with 637 atoms.

References

[1] G. Albrecht, An algorithm for parametric quadric patch construction, Computing **72** (2004) 1-12.

[2] G. Brunnett, Geometric design with trimmed surfaces, Computing Supplementum **10** (1995) 101-115.

[3] E. Cances, B. Mennucci, New applications of integral equations methods for solvation continuum models: ionic solutions and liquid crystals, J. Math. Chemistry **23** (1998) 309-326.

[4] A. Cohen, W. Dahmen, R. DeVore, Adaptive wavelet methods for elliptic operator equations-convergence rates, Math. Comp. **70** (2000) 27-75.

[5] M. Connolly, Molecular surface guide, 2006 (http://connolly.best.vwh.net).

[6] H. Coxeter, S. Greitzer, Geometry revisited, Random house: the L. W. Singer Company, New York, 1967.

[7] S. Dahlke, I. Weinreich, Wavelet-Galerkin-methods: an adapted biorthogonal wavelet basis, Constr. Approx. **9** (1993) 237-262.

[8] W. Dahmen, A. Kunoth, Adaptive wavelet methods for linear–quadratic elliptic control problems: convergence rates, SIAM J. Contr. Optim. **43**(5) (2005) 1640-1675.

[9] W. Dahmen, A. Kunoth, K. Urban, Biorthogonal spline wavelets on the interval: stability and moment conditions, Appl. Comput. Harmon. Anal. **6**, No. 2 (1999) 132–196.

[10] C. de Boor, A practical guide to splines, Springer-Verlag, New York, 1978.

[11] R. Dietz, J. Hoschek, B. Jüttler, An algebraic approach to curves and surfaces on the sphere and on other quadrics, Comput. Aided Geom. Des. **10**, No. 3-4 (1993) 211–229.

[12] R. Dietz, J. Hoschek, B. Jüttler, Rational patches on quadric surfaces, Comput.-Aided Des. **27**, No. 1 (1995) 27–40.

[13] G. Farin, S. Hahmann, G. Brunnett, in: Geometric Modelling, Dagstuhl 2002, Computing **72**, Wien, 2004, pp. 1–246.

[14] A. Forrest, On Coons and other methods for the representation of curved surfaces, Comput. Graph. Img. Process. **1** (1972) 341–359.

[15] W. Gordon, C. Hall, Construction of curvilinear co-ordinate systems and applications to mesh generation, Int. J. Numer. Methods Eng. **7** (1973) 461–477.

[16] M. Griebel, S. Knapek, G. Zumbusch, Numerical simulation in molecular dynamics, Springer, Berlin, 2007.

[17] W. Hackbusch, Integral equations: theory and numerical treatment, International series of numerical mathematics 120, Basel, Birkhaüser, 1995.

[18] W. Hackbusch, C. Lage, S. Sauter, On the efficient realization of sparse matrix techniques for integral equations with focus on panel clustering, cubature and software design aspects, in: Proc. final conf. of priority research programme boundary element methods, Stuttgart, 1997, pp. 51–75.

[19] H. Harbrecht, R. Schneider, Biorthogonal wavelet bases for the boundary element method, Math. Nachr. **269-270** (2004) 167–188.

[20] J. Hoschek, D. Lasser, Fundamentals of computer aided geometric design, A.K. Peters, Wellesley, 1993.

[21] Q. Hu, G. Wang, Necessary and sufficient conditions for rational quartic representation of conic sections, J. Comput. Appl. Math. **203** No. 1 (2007) 190-208.

[22] A. Kunoth, Adaptive wavelet schemes for an elliptic control problem with Dirichlet boundary control, Numer. Algor. **39** (1-3) (2005) 199-220.

[23] P. Laug, H. Borouchaki, Molecular surface modeling and meshing, in: Proc. 10th international meshing roundtable of Sandia national laboratory, 2001, pp. 31–41.

[24] L. Piegl, W. Tiller, The NURBS book, Springer, Berlin, 1995.

[25] M. Pratt, Cyclides in computer aided geometric design, Computer Aided Geometric Design **7** (1990) 221–242.

[26] H. Prautzsch, W. Boehm, M. Paluszny, Bézier and B-Spline techniques, Springer, Berlin, 2002.

[27] M. Randrianarivony, Geometric processing of CAD data and meshes as input of integral equation solvers, PhD thesis, Technische Universität Chemnitz, 2006.

[28] M. Randrianarivony, A survey on global continuity in geometric processing of CAD objects for the Wavelet-Galerkin scheme (in preparation).

[29] M. Sanner, A. Olsen, J. Spehner, Reduced surface: an efficient way to compute molecular surfaces, Biopolymers **38** (3) (1996) 305-320.

[30] R. Schneider, Multiskalen- und Wavelet-Matrixkompression: Analysisbasierte Methoden zur Lösung grosser vollbesetzter Gleichungssysteme, Teubner, Stuttgart, 1998.

[31] G. Schulze, Blending-Function-Methoden im CAGD, Diplomarbeit, Universität Dortmund, 1986.

[32] G. Schulze, Segmentation operators on Coons' patches, in: Mathematical methods in computer aided geometric design, edts. T. Lyche, L. Schumaker, Academic Press, Boston, 1989, pp. 561–572.

[33] G.-J. Wang, G.-Z. Wang, The rational cubic Bézier representation of conics. Computer Aided Geometric Design **9** (1992) 447–455.

[34] D. Whitley, Van der Waals graphs and molecular shape. J. Math. Chem. **23** (3-4) (1998) 377-397.